Journal of Physics: Conference Series **222** (2010) 012032 doi:10.1088/1742-6596/222/1/012032

Gravitational-wave signature of a thin-shell gravastar

Paolo Pani

E-mail: paolo.pani@ca.infn.it
Dipartimento di Fisica, Università di Cagliari, and INFN sezione di Cagliari, Cittadella Universitaria 09042 Monserrato, Italy

Emanuele Berti

E-mail: berti@phy.olemiss.edu
Department of Physics and Astronomy, The University of Mississippi, University, MS 38677-1848, USA
Theoretical Astrophysics 350-17, California Institute of Technology, Pasadena, CA 91125, USA

Vitor Cardoso

E-mail: vitor.cardoso@ist.utl.pt
Department of Physics and Astronomy, The University of Mississippi, University, MS 38677-1848, USA
Centro Multidisciplinar de Astrofísica - CENTRA, Dept. de Física, Instituto Superior Técnico, Av. Rovisco Pais 1, 1049-001 Lisboa, Portugal

Yanbei Chen, Richard Norte

E-mail: yanbei@tapir.caltech.edu, norte@caltech.edu
Theoretical Astrophysics 350-17, California Institute of Technology, Pasadena, CA 91125, USA

Abstract. We discuss how the emission of gravitational waves by ultra-compact objects can be qualitatively different depending on the presence or absence of an event horizon. Our case study are nonrotating thin-shell gravastars. The model has an infinitely thin shell with finite tension separating a de Sitter interior and a Schwarzschild exterior. The shell can be located arbitrarily close to the would-be event horizon, so a gravastar might seem indistinguishable from a black hole when tests are only performed on its external metric. We discuss gravitational perturbations of thin-shell gravastars and show that the spectrum of axial and polar quasinormal modes is completely different from that of a Schwarzschild black hole, even in the limit when the surface redshift becomes infinite. Furthermore, we study gravitational wave emission from the quasi-circular extreme mass ratio inspiral of compact objects of mass m_0 into massive thin-shell gravastars of mass $M \gg m_0$. The power radiated in gravitational waves during the inspiral shows distinctive peaks corresponding to the excitation of the polar oscillation modes of the gravastar. The frequency of these peaks usually depends on the equation of state, but for ultra-compact gravastars it typically lies within the optimal sensitivity bandwidth of LISA, providing a very specific signature of the horizonless nature of the central object.

Journal of Physics: Conference Series **222** (2010) 012032 doi:10.1088/1742-6596/222/1/012032

1. Introduction

One of the most elusive properties characterizing black holes (BHs) in general relativity is the presence of an event horizon. Evidence supporting the astrophysical reality of BHs necessarily depends on direct or indirect observations of an event horizon in astrophysical ultra-compact objects [1, 2]. Astrophysical observations usually probe the weak-gravity region, i.e. the space-time far away from the event horizon. The most precise measurements so far indicates the presence of a "dark object" of mass $M \simeq (4.1 \pm 0.6) \times 10^6 M_\odot$ in our own galaxy [3]. Recent millimeter and infrared observations of Sagittarius A*, the compact source of radio, infrared and X-ray emission at the center of the Milky Way, infer an intrinsic diameter of 37^{+16}_{-10} microarcseconds, which is even *smaller* than the expected apparent size of the event horizon of the presumed BH [4]. Traditional electromagnetic astronomy can at best yield lower limits on the gravitational redshift corresponding to hypothetical surfaces replacing the event horizon, and indeed some hold the view that an observational proof of the existence of event horizons based on electromagnetic observations is basically impossible (but see [1, 2, 5] for different viewpoints on this delicate issue). For this reason studies of the gravitational radiation signatures of event horizons, possibly probing the strong-gravity region, are necessary to confirm or disprove the BH paradigm [5, 6].

Gravitational-wave detectors offer a new way of observing BHs, complementing the wealth of information from present electromagnetic observations [7, 8]. A promising approach consists in probing the structure of compact objects which is encoded in their free oscillation spectrum, i.e. in their quasinormal modes (QNMs) [9]. Measuring several free oscillation frequencies, and comparing them with the QNM spectrum of BHs, provides a promising method to discern between BHs and horizonless objects [10]. These tests are one of the main goals of the Laser Interferometer Space Antenna (LISA) and they require a signal-to-noise ratio which may be even achieved by advanced Earth-based gravitational-wave interferometers [11, 12, 13].

In this paper we review some recent results in testing possible alternatives to the BH paradigm, following Refs. [14, 15]. We discuss compact objects whose external metric is virtually identical to that of a Schwarzschild BH, but which do not possess an event horizon. We focus on one of the simplest exemplars of such ultracompact horizonless objects: nonrotating thin-shell gravastars [16, 17]. We investigate their complete linearized dynamics, generalizing previous results [17, 18] by considering the thin-shell as a dynamical entity. Gravitational perturbations are generically discontinuous across the shell, due to a finite tension, and suitable matching conditions between interior and exterior perturbations have to be imposed [14]. By applying this general formalism, we discuss the QNM spectrum of a thin-shell gravastar. The spectrum of both axial and polar modes is complex and profoundly different from that of a BH, mainly because of the different boundary conditions at the surface replacing the event horizon. In particular polar modes depend on the equation of state (EOS) of matter on the shell and they can be used to discern between different gravastar models.

Furthermore polar modes can be excited during the inspiral of compact objects in quasi-circular orbits around stars [19, 20]. Thus differences between the QNM spectrum of an horizonless object and that of a BH correspond to a different gravitational signal emitted by the orbiting object because of the resonant scattering of gravitational radiation. We discuss gravitational-wave emission from the quasi-circular extreme mass ratio inspiral of compact objects of mass m_0 into massive thin-shell gravastars of mass $M \gg m_0$ [15]. As expected, the power radiated in gravitational waves during the inspiral shows distinctive peaks corresponding to the excitation of the polar oscillation modes of the gravastar.

The plan of the paper is as follows. In Sec. 2 we study free gravitational perturbations of a thin-shell gravastar, discussing matching conditions across the shell and reviewing the QNM spectrum. In Sec. 3 we discuss how the perturbation functions outside the shell (as obtained by the matching conditions) can be used to compute the gravitational-wave emission from the

quasi-circular extreme mass ratio inspiral of a point-like mass into a massive thin-shell gravastar. We conclude by discussing results and possible extensions of our work.

2. Gravitational perturbations of thin-shell gravastars

Let us start with the equilibrium model, which is a static thin-shell gravastar described by the metric [16, 17]

$$ds_0^2 = -f(r)dt^2 + \frac{1}{h(r)}dr^2 + r^2(d\theta^2 + \sin^2\theta d\varphi^2)\,, \tag{1}$$

with

$$f(r) = \begin{cases} h = 1 - \dfrac{2M}{r}\,, & r > a\,, \\ \\ \alpha\, h = \alpha\left(1 - \dfrac{8\pi\rho}{3}r^2\right)\,, & r < a\,, \end{cases} \tag{2}$$

where M is the gravastar mass and $\rho \equiv 3M/(4\pi a^3)$ is the "energy density" of the interior region. Junction conditions require the induced metric to be continuous across the shell, at $r = a$. This implies that also $f(r)$ has to be continuous at $r = a$, i.e. $\alpha = 1$. The metric above reduces to the de Sitter metric in the region $r < a$ and to the Schwarzschild metric for $r > a$. On the shell we must impose Israel's junction conditions [21] between the extrinsic curvature K_{ij} and the surface-energy tensor S_{ij}, i.e. $[[K_{ij}]] = 8\pi\,[[S_{ij} - \gamma_{ij}S/2]]$. Here and in the following we adopt the same index notation as in Ref. [14]. The symbol "[[...]]" denotes the "jump" of a given quantity across the shell, i.e. the difference between the limits of the corresponding quantity as $r \to a_\pm$. The surface energy Σ and surface tension Θ are then related to discontinuities in the metric coefficients as [16]

$$[[\sqrt{h}]] = -4\pi a\Sigma\,, \quad \left[\left[f'\sqrt{h}/f\right]\right] = 8\pi(\Sigma - 2\Theta)\,. \tag{3}$$

The QNM spectrum of thin-shell gravastars has been studied in great detail in Ref. [14] using the Regge-Wheeler (RW) gauge [22] (see also [17] for the axial QNM spectrum of five-layer gravastar models). In the RW gauge, perturbations split into two independent sets: two *axial* functions, usually called h_0 and h_1 and four *polar* functions, $H_0\,, H_1\,, H_2\,, K$. Axial and polar perturbations can be recast into two single functions, the so-called RW and Zerilli functions respectively. Here we briefly review the method developed in [14], which consists in matching perturbations in the de Sitter interior with perturbations in the Schwarzschild exterior. The matching procedure is performed by using Israel's junction conditions.

In the de Sitter interior, *both* the RW and Zerilli functions are described by the following analytical solution of the linearized equations [14]

$$\Psi^{\rm in} = r^{l+1}\left(1 - C\left(\frac{r}{2M}\right)^2\right)^{-i\frac{2M\omega}{2\sqrt{C}}} F\left(\frac{l+2-i\frac{2M\omega}{\sqrt{C}}}{2}, \frac{1+l-i\frac{2M\omega}{\sqrt{C}}}{2}, l+\frac{3}{2}, C\left(\frac{r}{2M}\right)^2\right)\,, \tag{4}$$

where $C \equiv (2M/a)^3 = 8\mu^3$ and $F(a,b,c,z)$ is the hypergeometric function. In obtaining the solution above, one must require regularity at the center ($r = 0$). For a thin-shell gravastar the surface stress-energy tensor Θ is, in general, nonvanishing. This implies that the perturbation functions are discontinuous across the shell. For axial perturbations these matching conditions read [14]

$$[[h_0]] = 0\,, \quad \left[\left[\sqrt{h}h_1\right]\right] = 0\,. \tag{5}$$

For a thin-shell gravastar Eqs. (5) just imply continuity of the RW function across the shell. In the polar case, the matching of interior and exterior perturbations at the gravastar shell

requires a more careful analysis because (unlike axial perturbations) polar perturbations of spherical objects actually induce motions of matter, which in turn couples back to gravitational perturbations. In Ref. [14] the following relations for the jump of the polar metric functions across the shell have been derived:

$$[[K]] = 0\,, \quad [[K']] = -8\pi \frac{\delta\Sigma}{\sqrt{f(a)}}\,,$$
$$\frac{2M}{a^2}\,[[H]] - [[H\,f']] - 2f(a)[[H']] + 4i\omega[[H_1]] = 16\pi\sqrt{f(a)}(1+2v_s^2)\delta\Sigma\,. \tag{6}$$

The parameter v_s depends on the EOS on the thin shell, $\Theta = \Theta(\Sigma)$:

$$v_s^2 \equiv -\left(\frac{\partial\Theta}{\partial\Sigma}\right)_{\Sigma=0}\,, \tag{7}$$

and it has the dimensions of a velocity. Roughly speaking, this parameter is related to the sound speed on the shell, although it is not necessarily bounded by $0 < v_s^2 < 1$ [23].

From Eq. (6) it is clear that polar QNMs (unlike axial QNMs) should depend on v_s, i.e. on the equation of state on the shell. This is a new feature that does not arise in the case of axial perturbations [17]. The situation closely parallels the ordinary stellar perturbation problem [24, 25]. The role played by the equation of state in the dynamical stability of gravastars against *spherically symmetric* perturbations was discussed in Ref. [16]. Our calculations extend that investigation to nonradial oscillations (see also Ref. [26] for a discussion on stability of thin-shells surrounding a BH).

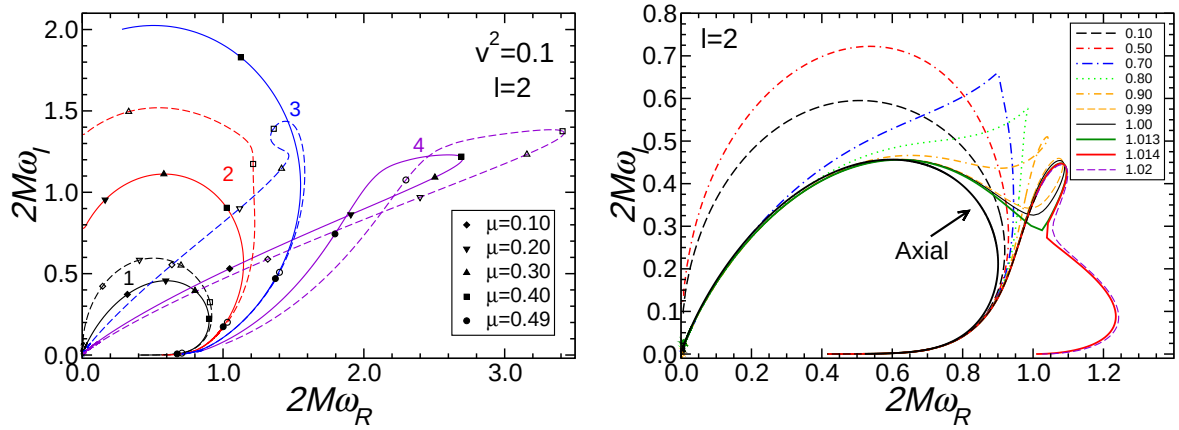

Figure 1. Left: Some axial (continuous lines) and polar (dashed lines) QNMs of a thin-shell gravastar with $v_s^2 = 0.1$ and $l = 2$ as the compactness μ varies. Numbers next to the polar and axial modes refer to the overtone index N ($N = 1$ being the fundamental mode). Right: Tracks of the fundamental polar and axial modes for different values of the "sound speed" parameter v_s when $v_s^2 > 0$. Figures are taken from Ref. [14].

2.1. QNM Spectrum

Here we briefly review results obtained in Ref. [14] for the QNM spectrum of thin-shell gravastars. We focus of $l = 2$ modes, although qualitatively similar results hold for $l > 2$. Axial and polar QNM frequencies have been computed by using the junction conditions (5) and (6) and the continued fraction method [27]. Some QNMs of a static thin-shell gravastar are shown in Fig. 1.

The QNM spectrum is qualitatively similar to that of 'ordinary" ultracompact stars (compare Fig. 1 with those in Refs. [28, 29]). For numerical calculations we first choose to keep v_s fixed and to vary μ from some starting value. In the left panel of Fig. 1 we chose $v_s^2 = 0.1$, and we computed the QNM spectrum for $\mu = 0.4$ by using the continued fraction method. We then follow each QNM as $\mu \to 0$ and as $\mu \to 1/2$ to produce the tracks displayed in the figure. The imaginary part of both axial modes (continuous lines) and polar modes (dashed lines) becomes very small in the "Schwarzschild limit", i.e. as $\mu \to 1/2$. Of course this method does not allow to find QNMs which do not exist when $\mu = 0.4$, but otherwise exist for smaller (or larger) compactness. Thus we choose different starting values of μ, in order to cover the entire spectrum.

Numerical results are in excellent agreement with previous results [17, 18] for axial modes. A new feature emerging in our case is that, unlike axial modes, polar modes depend on the EOS. In the right panel of Fig. 1 we show the tracks described in the complex plane by the fundamental polar and axial mode as we vary the compactness parameter μ and for different positive values of v_s^2. Although not shown, when $v_s^2 < 0$ polar modes are qualitatively similar to the axial ones.

One of the most important conclusions is that *neither axial nor polar modes of a gravastar reduce to the QNMs of a Schwarzschild BH when* $\mu \to 1/2$. In this limit, the real part of most modes is extremely small (much smaller than the Schwarzschild result, $2M\omega_R \simeq 0.74734$ for the fundamental mode with $l = 2$ [7]). Indeed, the QNM spectrum is drastically different from the QNM spectrum of a Schwarzschild BH: when $\mu \to 1/2$ the entire spectrum seems to collapse towards the origin. This is in sharp contrast with the Schwarzschild BH case and it can be used to tell very compact gravastars from BHs [17].

The dependence of polar QNMs on the EOS as shown in the right panel of Fig. 1 is quite interesting. For small values of the sound speed parameter ($v_s^2 \leq 0.5$ or so) the modes show an ordinary behavior, which is similar to that (not shown) for $v_s^2 < 0$ and to that for axial modes. However for larger values modes have a peculiar behavior, until a critical value $v_{\rm crit} \simeq 1.007$ is reached and, for $v_s > v_{\rm crit}$, the QNM behavior changes quite drastically.

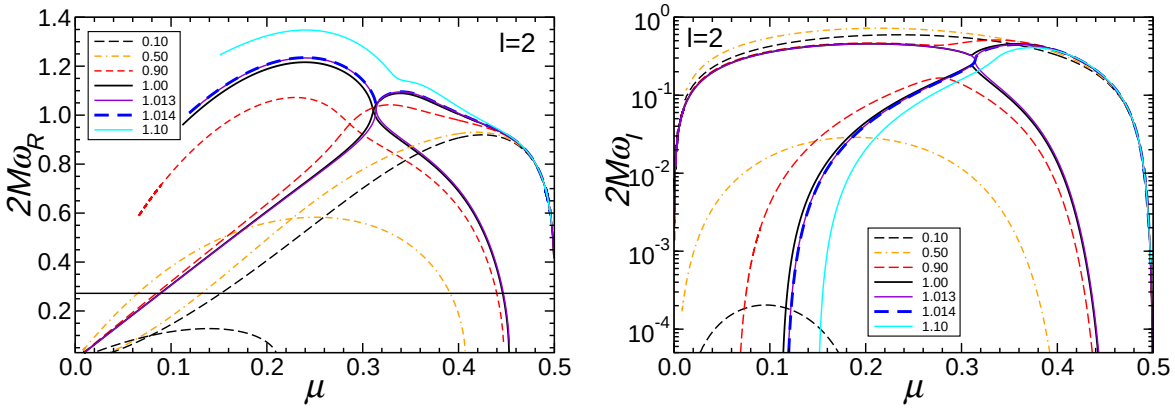

Figure 2. Real (left) and imaginary parts (right) of the fundamental polar mode for different values of the equation of state parameter v_s. For each (μ,v_s) a couple of mode exists, which is shown with the same linestyle. The horizontal line in the left panel corresponds to twice the orbital frequency of a particle in circular orbit at the innermost stable circular orbit (ISCO): only modes below the line can be excited during a quasicircular inspiral (cfr. Sect. 3). Figures are taken from Ref. [14].

Even more interestingly, when $v_s^2 > 0$ the QNM spectrum has a very rich and complex structure. A *second* family of QNMs with very small imaginary part appears. In the left (right) panel of Fig. 2 we show the real (imaginary) part of both the first and the second

family of modes, for some selected values of v_s. The second family of QNMs has very long damping, and in this sense it is similar to the s-modes of "ordinary" ultra-compact stars discussed by Chandrasekhar and Ferrari [25], although for gravastars these modes appear for *small* compactness $\mu < \mu_{\rm crit}(v_s, l)$. These mode are suitable to be computed also by the resonant method [25, 30] whose results are in excellent agreement with the continued fraction method. The imaginary part of modes with $v_s^2 \gtrsim 0.84$ rapidly approaches zero at some finite compactness μ while the real part of the modes stays finite. This suggests an instability at high v_s, as shown by the critical threshold in Fig. 3. In the region below the solid line, thin-shell gravastars may undergo an instability to nonradial perturbations with $l = 2$. Moreover the dashed line in Fig. 3 corresponds to the critical line above which the second family of modes disappears (both the real and imaginary part of modes tend to zero).

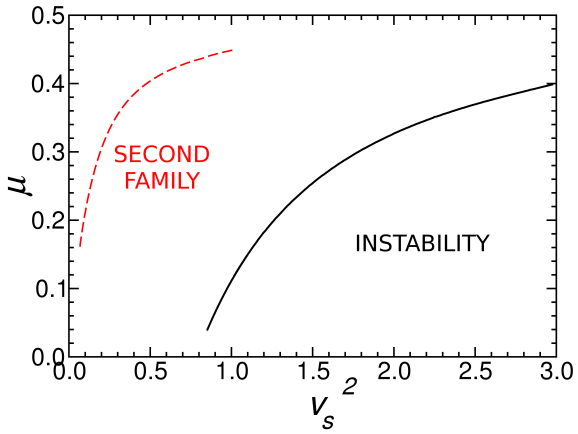

Figure 3. Significant thresholds in the $(\mu,\, v_s^2)$ plane. Numerical results suggest that the region below the black solid line corresponds to unstable thin-shell gravastar models. The second family of modes exists in the region of parameter below the red dashed line (see the text for a detailed discussion). Figures are taken from Ref. [14].

3. Gravitational-wav emission from extreme mass ratio inspirals

Here we consider a physical process where the GW energy spectrum has distinct signatures depending on whether the dynamics involve a thin-shell gravastar or a BH. We review recent results in Ref. [15], in which the gravitational emission by a particle with mass m_0 orbiting a horizonless object with mass $M \gg m_0$ has been computed in detail (see Refs. [19, 20, 31] for related works considering neutron stars). We consider a particle orbiting a thin-shell gravastar in a circular orbit with radius R_0. This should be sufficient to show that gravitational radiation from extreme mass ratio inspirals around horizonless objects is drastically different from the BH case. Similar arguments can presumably be made for more complex (or contrived) gravastar models and for eccentric orbits.

The time-averaged energy-flux can be shown to be [19, 15]

$$\dot{E}^R(m\omega_K) \equiv \left\langle \frac{dE_{GW}}{dt} \right\rangle = \sum_{lm} \frac{m_0^2}{4\pi(m\omega_K)^2}\, |\hat{A}_{lm}(m\omega_K)|^2 \equiv \sum_{lm} \dot{E}^R_{lm}. \tag{8}$$

where the dot indicates differentiation with respect to proper time, E is the energy per unit mass of the particle, $\omega_{\rm K} = \sqrt{M/R_0^3}$ denotes the Keplerian orbital frequency and $(l,\, m)$ are the usual quantum numbers. As discussed in detail in Ref. [19], the function $\hat{A}_{lm}(\omega)$ is related to the amplitude of the wave at radial infinity apart a Dirac delta contribution, $\delta(\omega - m\omega_K)$,

and it can be computed in terms of two independent solutions Ψ^0_{lm} and Ψ^1_{lm} of the following inhomogeneous Bardeen-Press-Teukolsky (BPT) equation [32, 33]

$$\left\{\Delta^2\frac{d}{dr}\left[\frac{1}{\Delta}\frac{d}{dr}\right]+\left[\frac{\left(r^4\omega^2+4i(r-M)r^2\omega\right)}{\Delta}-8i\omega r-2n\right]\right\}\Psi_{lm}(\omega,r)=-T_{lm}(\omega,r), \quad (9)$$

satisfying suitable boundary conditions [31]. In the equation above $\Delta=r^2-2Mr$ and the source term $T_{lm}(\omega,r)$ describes the point mass m_0 moving on a given orbit around the gravastar. In order to evaluate Ψ^0_{lm} and Ψ^1_{lm}, the BPT equation is integrated with an adaptive Runge-Kutta method starting with initial conditions on the gravastar shell obtained from the Zerilli and RW functions (as well as their derivatives), which can be constructed from the interior perturbations, Eq. (4), by using the junction conditions Eqs. (5)-(6) (see [15] for details).

The energy flux emitted in gravitational waves $\dot{E}^R$, normalized by the Newtonian quadrupole energy flux $\dot{E}^N$, reads

$$P(v)\equiv\frac{\dot{E}^R}{\dot{E}^N}=\sum_{lm}\frac{5}{128\pi}\frac{M^2}{(m\omega_K)^2v^{10}}|\hat{A}_{lm}(m\omega_K)|^2\,. \quad (10)$$

where $\dot{E}^N=32m_0^2v^{10}/(5M^2)$, $v=(M\omega_K)^{1/3}=p^{-1/2}$ being the orbital velocity and $p=R_0/M$ the semilatus rectum of the circular orbit. The normalized energy flux (10) can be computed up to $v\leq 1/\sqrt{6}\simeq 0.408$, which corresponds to the innermost stable circular orbit (ISCO) at $R_0=6M$. The instability of circular orbits with $R_0<6M$ sets an upper bound on the velocity of the point mass. If the radius of the gravastar is larger than the ISCO, i.e. $\mu<0.1666$, the upper limit in v is smaller. From the analytical form of the stress-energy tensor in Eq. (9) (see also [19]) it is easy to see that, for each assigned l, a mode of the star is excited when the orbital frequency satisfies the resonant condition

$$m\omega_{\rm K}=\omega_{\rm QNM}\,, \quad (11)$$

where $\omega_{\rm QNM}$ is the QNM frequency. Thus we expect sharp peaks to appear at the values of v corresponding to the excitation of the gravastar QNMs for different values of the angular momentum parameter l. This offers an intriguing signature of the absence of event horizons, since the emitted power for a Schwarzschild BH does not show any peak. In fact one can easily check that the frequency of the fundamental QNM of a Schwarzschild BH is *higher* than the critical value $m\omega_{\rm K}$ corresponding to a particle at the ISCO [31]. In other words, Schwarzschild QNMs can only be excited by particles plunging into the BH, while the QNMs of a gravastar can be excited *during the inspiral*.

3.1. Comparing the gravitational flux of a thin-shell gravastar and of a black hole

Our purpose here is to compare and contrast the energy flux from particles orbiting Schwarzschild BHs to the energy flux from particles orbiting thin-shell gravastars. The gravitational emission of a Schwarzschild BH perturbed by a particle has been studied analytically and numerically in great detail for both circular and eccentric orbits [34, 35, 36]. We consider thin-shell gravastars as a case study for generic compact horizonless objects, but several different models can be explored (see e.g. [16, 17]). However we expect the qualitative results of our analysis to apply quite in general, since the main difference in the gravitational-wave emission of a compact object comes from the different boundary conditions at the "surface" replacing the BH event horizon, rather than from the specific nature of this surface.

The numerical study in Ref. [15] covers the whole range in compactness ($0<\mu<0.5$) and it mainly focuses on the most physical range of the EOS parameter ($0<v_s^2<1$), although the

superluminal case ($v_s^2 > 1$) and models with $v_s^2 < 0$ were also investigated. For each value of the gravastar parameters (μ, v_s^2) we integrate the perturbations equations for a point-like object of mass m_0 moving on a circular orbit of radius R_0 with orbital velocity v and we compute the energy flux (10) by using the BPT formalism, as previously discussed.

As shown in Section 2, in the Schwarzschild limit $\mu \to 0.5$ the real part of the QNM frequency tends to zero and to a very good approximation it is independent of v_s [14]. In order for a QNM to be excited by particles in circular orbits, the QNM frequency must be small enough to allow for the resonant condition (11).

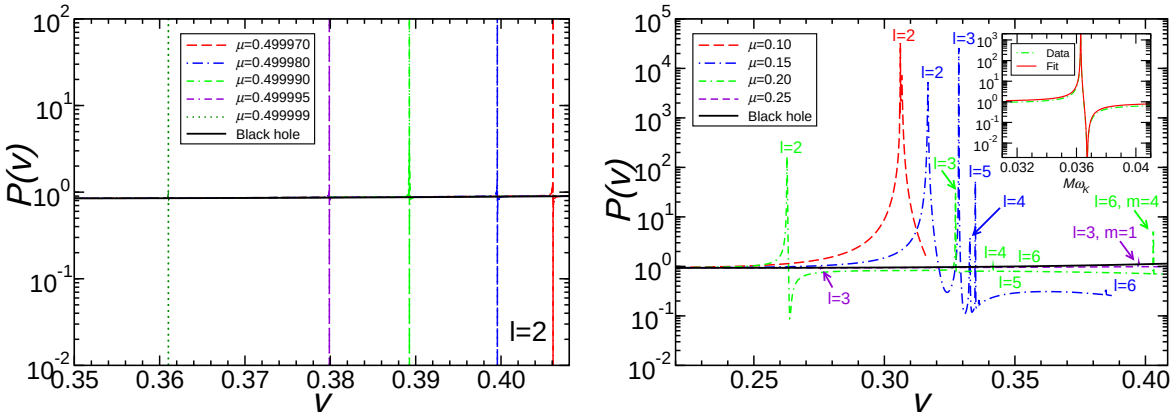

Figure 4. Left: Dominant ($l = 2$) contribution to the energy flux for very high compactness and $v_s^2 = 0.1$ (but when $\mu \sim 0.5$ resonances are almost independent on v_s^2). Right: Energy flux (summed up to $l = 6$) of the gravitational radiation emitted by a small mass orbiting thin-shell gravastars with $v_s^2 = 0.1$ and different values of μ, compared with the flux for a Schwarzschild BH, as a function of the particle orbital velocity v. In the inset a typical resonance is plotted.The comparison between numerical data and a simple harmonic oscillator [20] is shown. Figures are taken from Ref. [15].

In Fig. 4 we show the energy flux for a gravastar. In the left panel the dominant ($l = 2$) contribution at very high compactness is shown. The frequencies of the lowest QNMs of a Schwarzschild BH are higher than those of an ultra-compact gravastar, and cannot be excited by particles in stable circular orbits. For this reason the power emitted by a BH (on the scale of the plot) appear almost as a flat line. Resonance peaks do appear for gravastars, as expected, when $\omega_{\rm QNM} = 2\omega_{\rm K}$. Notice that these resonances are extremely narrow and they would get even narrower for $l > 2$. This is because the imaginary part of the excited modes is extremely small ($2M\omega_I \sim 10^{-7}$, 10^{-10} for $l = 2$ and $l = 3$, respectively) in the high-compactness limit $\mu \to 0.5$, leading to a corresponding decrease in the quality factor of the oscillations. Whether these resonances are actually detectable is an interesting question for LISA data analysis [31].

In Table 1 we list the expected excited modes, as extracted from the QNM spectrum for different values of μ corresponding to ultra-compact gravastars. Both for $l = 2$ and for $l = 3$ the typical frequencies lay within the optimal sensitivity bandwidth of LISA, providing a very specific signature of the horizonless nature of the central object. A simple fit of the resonant frequency as a function of the compactness suggests that LISA has the potential to reveal solid surfaces replacing horizons even when these solid surfaces are extremely close to the location of the Schwarzschild horizon [15].

The rich structure of the QNM spectrum allows gravastars which are as compact as neutron stars to leave a signature on the gravitational signal emitted by small, inspiralling compact objects. In the right panel of Fig. 4 we plot the normalized energy flux $P(v)$ as a function of the

Table 1. Values of the compactness μ, angular momentum quantum number l, QNM frequency, orbital velocity v and gravitational-wave frequency $\nu_{\rm GW}$ of the circular orbits which correspond to the excitation of the fundamental QNM of the gravastar for the given multipole. The Keplerian frequency is given in mHz and rescaled to the typical gravastar mass $M_6 = 10^6 M_\odot$ that would be targeted by LISA [15].

μ	l	$M\omega_{\rm QNM}$	v	$(M_6/M)\nu_{\rm GW}$ (mHz)
0.49997	2	0.1339	0.4061	4.328
	3	0.1508	0.3691	4.873
0.49998	2	0.1276	0.3996	4.123
	3	0.1429	0.3625	4.616
0.49999	2	0.1180	0.3893	3.812
	3	0.1310	0.3521	4.232
0.499995	2	0.1096	0.3799	3.543
0.499999	2	0.0941	0.3610	3.041

orbital velocity for gravastar models with $v_s^2 = 0.1$ and compactness in the range $0.1 \lesssim \mu \lesssim 0.25$, as well as for a Schwarzschild BH. The total flux was computed by adding all multipoles ($|m| \leq l$) and by truncating the multipolar expansion at $l = 6$. Roughly speaking, a truncation at $l = 6$ produces a relative error (in the non-resonant regime) of order $p^{-5} = v^{10}$ [19, 36]. When $\mu \gtrsim 0.166$ the ISCO is located outside the gravastar and the plots extend up to the ISCO velocity $v_{\rm ISCO} \simeq 0.408$ (corresponding to $R_0 = 6M$). For less compact gravastars the energy flux is truncated at the velocity corresponding to the location of the shell. When $l = 2$ and $v_s^2 = 0.1$ no QNMs can be excited for $0.21 \leq \mu \leq 0.49997$. In this compactness range the energy flux emitted by either the gravastar or the BH is mostly due to the orbital motion and it only depends on the compactness of the central object.

In the inset of Fig. 4 we zoom around a typical resonance as function of the Keplerian orbital frequency $M\omega_{\rm K}$ of the particle for $\mu = 0.2$ and $l = 2$ (dashed green line). A fit using the simple harmonic oscillator model of Ref. [20] (red line) reproduces the qualitative features of both resonance and antiresonance.

The complex structure of the spectrum for values of μ smaller than about 0.2 is best understood by considering the real and imaginary parts of the weakly damped QNM frequencies of a gravastar as plotted in the left and right panels of Fig. 2, respectively. Only QNMs whose real part lies *below* the horizontal line in the left panel (corresponding to twice the ISCO orbital frequency for a particle in circular orbit) can be excited. The range of μ over which QNMs can be excited depends on the speed of sound parameter v_s and on l.

4. Conclusions

We have discussed in detail gravitational perturbations of a thin-shell gravastar, a model which is representative of generic horizonless ultra-compact objects. We have studied the QNM spectrum and showed that both axial and polar modes are drastically different from Schwarzschild QNMs, even when the compactness approaches the Schwarzschild value, $\mu \to 0.5$. In particular polar modes depend on the equation of state of matter on the thin-shell and they may be used to discern between different gravastar models. More importantly, polar modes can be excited by small masses orbiting the thin-shell gravastar. We have discussed point-like particles in circular orbit and we have shown that for some orbital frequencies the energy flux in GWs shows resonances. The existence of resonant frequencies depends both on the compactness and on the equation of state on the shell. However, in the most interesting case of ultra-compact gravastars ($\mu \to 0.5$) resonant frequencies are independent on the EOS and above a certain critical compactness resonances always exist. Interestingly enough, typical resonant frequencies lay within the optimal sensitivity bandwidth of LISA, providing a very specific signature of the horizonless nature of the central object. It would be interesting to generalize our method to

more realistic models for horizonless objects [16, 17], possibly in connection with both circular and eccentric inspirals. Another interesting and nontrivial development is the generalization to the case of rotating gravastars [37, 38].

Acknowledgements
This work was partially supported by FCT - Portugal through projects PTDC/FIS/64175/2006, PTDC/FIS/098025/2008 and PTDC/FIS/098032/2008. Y.C. was supported by NSF grants PHY-0653653 and PHY-0601459, and the David and Barbara Groce Start-up Fund at Caltech. E.B.'s research was supported by NSF grant PHY-0900735.

References

[1] R. Narayan, New J. Phys. **7**, 199 (2005)
[2] M. A. Abramowicz, W. Kluzniak and J. P. Lasota, Astron. Astrophys. **396**, L31 (2002)
[3] A. M. Ghez *et al.*, Astrophys. J. **689**, 1044 (2008)
[4] S. Doeleman *et al.*, Nature **455**, 78 (2008)
[5] M. Visser,
[6] W. Kundt, Gen. Rel. Grav. **41** (2009) 1967
[7] E. Berti, V. Cardoso and A. O. Starinets, Class. Quant. Grav. **26**, 163001 (2009)
[8] F. D. Ryan, Phys. Rev. D **52**, 5707 (1995).
[9] K. D. Kokkotas and B. G. Schmidt, Living Rev. Rel. **2**, 2 (1999)
[10] O. Dreyer et *al.*, Class. Quant. Grav. **21**, 787 (2004)
[11] E. Berti, V. Cardoso and C. M. Will, Phys. Rev. D **73**, 064030 (2006)
[12] E. Berti, J. Cardoso, V. Cardoso and M. Cavaglia, Phys. Rev. D **76**, 104044 (2007)
[13] B. S. Sathyaprakash and B. F. Schutz, Living Rev. Rel. **12**, 2 (2009)
[14] P. Pani, E. Berti, V. Cardoso, Y. Chen and R. Norte, arXiv:0909.0287 [gr-qc].
[15] P. Pani, E. Berti, V. Cardoso, Y. Chen and R. Norte, in preparation
[16] M. Visser and D. L. Wiltshire, Class. Quant. Grav. **21**, 1135 (2004)
[17] C. B. M. Chirenti and L. Rezzolla, Class. Quant. Grav. **24**, 4191 (2007)
[18] P. P. Fiziev, Class. Quant. Grav. **23**, 2447 (2006)
[19] L. Gualtieri, E. Berti, J. A. Pons, G. Miniutti and V. Ferrari, Phys. Rev. D **64**, 104007 (2001)
[20] J. A. Pons, E. Berti, L. Gualtieri, G. Miniutti and V. Ferrari, Phys. Rev. D **65**, 104021 (2002)
[21] W. Israel, Nuovo Cim. B **44S10**, 1 (1966) [Erratum-ibid. B **48**, 463 (1967 NUCIA,B44,1.1966)].
[22] T. Regge and J.A, Wheeler, Phys.Rev. **108**, 1063 (1957).
[23] M. Visser, 'Lorentzian wormholes: From Einstein to Hawking," *Woodbury, USA: AIP (1995) 412 p*
[24] S. Chandrasekhar and V. Ferrari, Proc. Roy. Soc. Lond. A **432**, 247 (1991).
[25] S. Chandrasekhar and V. Ferrari, Proc. Roy. Soc. Lond. A **434**, 449 (1991).
[26] P. R. Brady, J. Louko and E. Poisson, Phys. Rev. D **44** (1991) 1891.
[27] E. W. Leaver, Proc. Roy. Soc. Lond. A **402** (1985) 285.
[28] N. Andersson, Y. Kojima and K. D. Kokkotas, Astrophys. J. **462**, 855 (1996)
[29] N. Andersson, Gen. Rel. Grav. **28**, 1433 (1996).
[30] E. Berti, V. Cardoso and P. Pani, Phys. Rev. D **79** (2009) 101501
[31] E. Berti, J. A. Pons, G. Miniutti, L. Gualtieri and V. Ferrari, Phys. Rev. D **66** (2002) 064013
[32] J. M. Bardeen and W. H. Press, J. Math. Phys. **14**, 7 (1973).
[33] S. A. Teukolsky, Astrophys. J. **185**, 635 (1973).
[34] C. Cutler, D. Kennefick and E. Poisson, Phys. Rev. D **50**, 3816 (1994).
[35] E. Poisson, Phys. Rev. D **52**, 5719 (1995) [Addendum-ibid. D **55**, 7980 (1997)]
[36] N. Yunes and E. Berti, Phys. Rev. D **77**, 124006 (2008)
[37] V. Cardoso, P. Pani, M. Cadoni and M. Cavaglia, Phys. Rev. D **77** (2008) 124044
[38] C. B. M. Chirenti and L. Rezzolla, Phys. Rev. D **78**, 084011 (2008)